

## INVESTIGATION OF STRESS CONCENTRATION FACTORS IN COUNTERSUNK HOLES OF BIAXIALLY LOADED ISOTROPIC PLATES

Abdullah A. Jabri\* and Mohammad A. Gharaibeh

Department of Mechanical Engineering, The Hashemite University, Zarqa, 13133, JORDAN  
E-mail: 2034476@std.hu.edu.jo

This study employs finite element analysis (FEA) and response surface methodology (RSM) to analyze the stress concentration factor (SCF) in a biaxially loaded isotropic plate with a central countersunk hole. A finite element model is built using ANSYS and employed to generate stress concentration factor values. The finite element model was optimized in terms of mesh density and properties based on data from past literature. Five dimensionless parameters are studied: radius to width ratio, thickness to radius ratio, countersink to thickness ratio,  $\sigma_y$  to  $\sigma_x$  ratio and countersink angle. The effect of the different configurations was studied using RSM. Finally, a precise second order equation was produced to estimate the value of SCF with dimensionless parameters.

**Key words:** countersunk hole, finite element analysis, stress concentration factor, ANSYS, biaxial loading.

### 1. Introduction

Countersunk holes are commonly used in industrial and engineering joints such as riveting to join two thin plates and maintain a flush aerodynamic surface. The presence of such irregularities i.e. countersunk holes leads to stress concentrating on the thickness of the joined structures. This phenomenon is often described using stress concentration factor (SCF), which is mathematically defined as the ratio between the maximum stress value  $\sigma_{max}$  and nominal stress value  $\sigma_{nominal}$ .

$$K_t = \frac{\sigma_{max}}{\sigma_{nominal}}. \quad (1.1)$$

Several studies have been conducted to investigate the phenomenon of stress concentration around the holes. Pilkey and Pilkey [1] summarized existing literature on the subject, specifically on stress concentration in circular holes in thin plates under various loading conditions. Shivakumar and Newman [2] conducted a three-dimensional finite element analysis of the stress concentration factor in thin and thick plates with circular holes, considering diverse loading scenarios. Similarly, Wu and Mu [3] numerically examined SCF in isotropic and orthotropic plates having central circular holes subjected to uniaxial and biaxial loading. Kostouf *et al.* [4] examined the effects of plate thickness and Poisson's ratio on the in-plane stress concentration factor and the out-of-plane stress constraint factor. In contrast, Li *et al.* [5] explored how different notch configurations influence these stress concentration factors. Additionally, She *et al.* [6] used finite element methods to analyze how the thickness-to-root radius ratio and aspect ratio of elliptical holes affect stress concentration factors. Enab [7] explored SCF in elliptical holes, while Kumar *et al.* [8], Jadvani *et al.* [9], and Zhou and Fei [10] investigated various types of cutouts. Kumar *et al.* presented a literature review on stress concentration in composite panels with holes and cutouts [11].

Some papers were published discussing the SCF in plates with countersunk holes. Wharely [12] conducted experimental studies to assess the localized stresses in Aluminum plates. Cheng [13] utilized the stress

---

\* To whom correspondence should be addressed

freezing technique to find stress within the thickness of plates with countersunk holes. Cheng explored thirteen configurations with varying depths and countersink angles, conducting seven tests for specimens in tension loading and six for bending. His research indicated that the stress concentration is located at the edge of the countersink. Shivakumar *et al.* [14] and Bhargava and Shivakumar [15, 16] conducted extensive finite element analysis on isotropic and orthotropic plates with countersunk holes. Intricate empirical equations based on FEA data to calculate the SCF for plates with countersunk holes in a uniaxial loading scenario were presented by Darwish *et al.* [17, 18]. Gharaibeh [19] presented a study on the stress concentration factor in plates with double countersunk holes due to uniaxial tension. Gharaibeh *et al.* [20] presented another paper that provided a more straightforward formula for SCF calculation and optimum hole geometries that minimize the SCF value.

Several studies [21-25] investigated the issue of strain concentration in countersunk holes in axial and biaxial loading scenarios, providing valuable equations and precise models.

Alshyyab and Darwish [26] presented a paper using FEA to find the effect of the biaxial stress ratio and the hole configuration and loading ratio on SCF. They found that the maximum SCF is located at the straight shank part of the hole.

Much research has been conducted on stress concentration in plates with various configurations; however, there is a notable gap in studies that explore the effects of different loading conditions, particularly in scenarios involving biaxial loading. This paper specifically addresses this gap by investigating the stress concentration factor (SCF) in plates featuring a single countersunk hole under biaxial loading conditions, a combination that has not been extensively studied.

This paper intends to employ the finite element method (FEM) and response surface method (RSM) to investigate the stress concentration factor (SCF) in biaxially loaded plates featuring a single countersunk hole. Moreover, it aims to develop a simple equation based on dimensionless variables for determining the SCF.

## 2. Geometry and load description

The system studied is an elastic plate with a countersunk hole placed centrally. The plate is subjected to biaxial loading, as illustrated in Fig.1. The geometric parameters shown include the plate length ( $l$ ), width ( $w$ ), and thickness ( $t$ ), which can be split into two parts: the countersink depth ( $C_s$ ) and the straight shank depth ( $b$ ) (hence,  $t = C_s + b$ ). Additionally, the shank radius ( $r$ ) and countersink angle ( $\theta_c$ ), which is usually between  $80^\circ$  and  $120^\circ$ , were specified. Also loading in the  $x$  and the  $y$  directions are shown ( $\sigma_x, \sigma_y$ ).

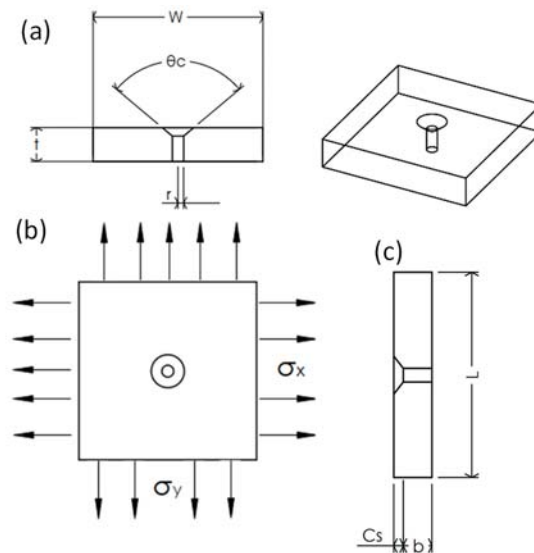


Fig.1. Plate configuration (a) X-Y plane, (b) X-Z plane, (c) Y-Z plane.

For the purpose of this study, we examined the effect of the following five nondimensional parameters: countersink angle ( $\theta_c$ ), thickness to radius ratio ( $t/r$ ), countersink depth to plate thickness ratio ( $C_s/t$ ), radius to width ratio ( $r/w$ ) and the ratio between ( $\sigma_y$ ) and ( $\sigma_x$ ) ( $\sigma_r = \sigma_y / \sigma_x$ ). For all cases the length to radius ratio was kept constant ( $l/r = 15$ ) which is done to eliminate the effect of plane length on SCF value.

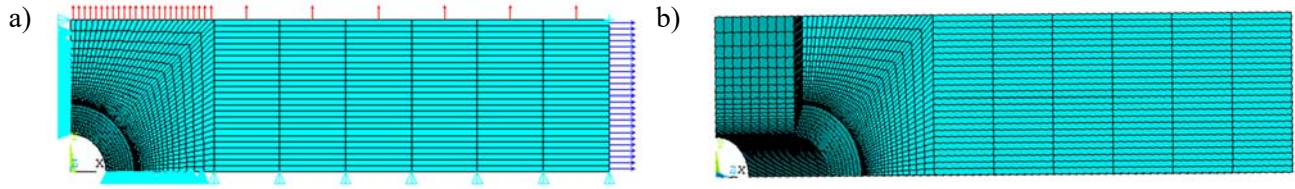


Fig.2. (a) Boundary conditions and loads applied on a quarter model, (b) finite element mesh.

### 3. Finite element modelling

As depicted in Fig.2. only a quarter of the whole plate was modeled because the geometry of the plate, loading and boundary conditions are symmetric. Hexahedron elements (SOLID 185) were employed to create the FE mesh. The origin is located the center of the hole and at ( $X=0, Y=0, Z=0$ ), on the planes ( $X=0, Y=0$ ) displacement is constrained to zero and displacement on the  $Z$  direction is also constrained to zero, biaxial load ( $\sigma_X = 1$  and  $\sigma_Y = \sigma_X \times \sigma_r$ ) is applied on the two planes ( $X=l, Y=w$ ). The plate is homogeneous and isotropic, with an elastic modulus ( $E = 200 \text{ GPa}$ ) and Poisson's ratio ( $\nu = 0.33$ ).

As shown in Fig.2b, the FE mesh is designed to have a higher density near the hole edges and gets lower everywhere else. This ensures high accuracy at the areas of interest while decreasing the time required to solve each iteration this was implemented from a previous study done by Gharaibeh *et al.* [20].

### 4. SCF analysis using RSM

Response surface method is a statistical and mathematical technique used to analyze the relationship between a set of independent variables and the response variable (SCF in this case). RSM is especially valuable when the relationships between the independent variables are complex and cannot be easily described by simple linear equations. RSM is usually used to fit a second order response surface. Also, RSM describes the main effects and interactions of the independent variables on the response variable while using the minimum number of runs.

For the purposes of this analysis MINITAB version 21.4.1 was used to design the response surface. Table 1 shows the five dimensionless variables countersink angle ( $\theta_c$ ), thickness to radius ratio ( $t/r$ ), countersink depth to plate thickness ratio ( $C_s/t$ ), radius to width ratio ( $r/w$ ) and the ratio between ( $\sigma_y$ ) and ( $\sigma_x$ ) ( $\sigma_r = \sigma_y / \sigma_x$ ) each of the variables is split into three levels: low ( $-1$ ), middle ( $0$ ) and high ( $+1$ ). A blocked full factorial ( $2^k$ ) central composite design (CCD) with central and axial points ( $2k$ ) where  $k$  is the number of independent dimensionless variables ( $k = 5$  for this study). In this design, 54 FE  $CCD = 2^k + 2k + 12$  the model was improved by adding 12 replicate runs at the central point to ensure the stability of the model as suggested by MINITAB (four runs of which were eliminated because of invalid geometry). To construct a second-order response surface, the following formula was taken into consideration:

$$K_t = c_o + \sum_{i=1}^k c_i Z_i + \sum_{i < j} \sum c_{ij} Z_i Z_j + \sum_{i=1}^k c_{ii} Z_{ii}^2 + e. \quad (4.1)$$

$Z_i$  and  $Z_j$  represent the independent variables,  $c_o$  denote the constant coefficient, and  $c_i$ ,  $c_{ii}$ , and  $c_{ij}$  represent the coefficients for linear and second-order terms respectively. Additionally,  $e$  represents the random relative error.

Table 1. The CCD for the five independent variables.

Independent variables	RSM levels		
	low (-1)	middle (0)	high (+1)
radius to width ratio ( $r/w$ )	0.1	0.25	0.4
thickness to radius ratio ( $t/r$ )	0.5	2.5	4.5
countersink depth to plate thickness ratio ( $C_s/t$ )	0.1	0.3	0.5
countersink angle ( $\theta_c$ )	80	100	120
ratio between ( $\sigma_y$ ) and ( $\sigma_x$ ) ( $\sigma_r = \sigma_y / \sigma_x$ )	0.5	2.5	4.5

## 5. Results and discussion

### 5.1. Central composite design results

After completing the fifty experimental runs the SCF outcomes were recorded as shown in Appendix 1, the highest SCF value was ( $K_t = 19.762$ ) the values for the independent variables are ( $r/w = 0.10$ , ( $t/r = 4.5$ , ( $C_s/t = 0.5$ , ( $\theta_c = 120$  and ( $\sigma_r = 4.5$ ). In all engineering applications we aim to reduce the SCF thus this configuration is not advisable.

### 5.2. Regression, analysis of variance and residual analysis

For the work presented in this paper the most accurate regression model for  $K_t$  is quadratic and includes all the independent variables as shown in the equation below:

$$\begin{aligned}
 K_t = & c_o + c_1 \left(\frac{r}{w}\right) + c_2 \left(\frac{t}{r}\right) + c_3 \left(\frac{C_s}{t}\right) + c_4 (\theta_c) + c_5 (\sigma_r) + c_{12} \left(\frac{r}{w}\right) \left(\frac{t}{r}\right) + c_{13} \left(\frac{r}{w}\right) \left(\frac{C_s}{t}\right) + \\
 & + c_{14} \left(\frac{r}{w}\right) (\theta_c) + c_{15} \left(\frac{r}{w}\right) (\sigma_r) + c_{23} \left(\frac{t}{r}\right) \left(\frac{C_s}{t}\right) + c_{24} \left(\frac{t}{r}\right) (\theta_c) + c_{25} \left(\frac{t}{r}\right) (\sigma_r) + c_{34} \left(\frac{C_s}{t}\right) (\theta_c) + \\
 & + c_{35} \left(\frac{C_s}{t}\right) (\sigma_r) + c_{45} (\theta_c) (\sigma_r) + c_{11} \left(\frac{r}{w}\right)^2 + c_{22} \left(\frac{t}{r}\right)^2 + c_{33} \left(\frac{C_s}{t}\right)^2 + c_{44} (\theta_c)^2 + c_{55} (\sigma_r)^2.
 \end{aligned} \quad (5.1)$$

After analyzing the data in Table 2, seven terms were removed from the equation to reduce complexity without affecting the accuracy of the model. This is because the contribution of the removed terms to the final result is insignificant. Therefore, the simplest yet accurate equation describing  $K_t$  is as presented below:

$$\begin{aligned}
 K_t = & 4.021 + 0.983\left(\frac{r}{w}\right) - 0.576\left(\frac{t}{r}\right) - 7.85\left(\frac{C_s}{t}\right) - 0.02296(\theta_c) + 0.616(\sigma_r) + \\
 & + 2.498\left(\frac{r}{w}\right)(\sigma_r) + 1.021\left(\frac{t}{r}\right)\left(\frac{C_s}{t}\right) + 0.00399\left(\frac{t}{r}\right)(\theta_c) + 0.0886\left(\frac{t}{r}\right)(\sigma_r) + \\
 & + 0.0662\left(\frac{C_s}{t}\right)(\theta_c) + 1.617\left(\frac{C_s}{t}\right)(\sigma_r) + 0.00544(\theta_c)(\sigma_r) + 0.1693(\sigma_r)^2.
 \end{aligned}
 \tag{5.2}$$

The  $R^2$  value for the equation comprising 14 terms is 99.64, signifying a high level of accuracy for the model.

The residuals (the error between the model and the FEA results) of the proposed model were checked. A valid RSM model demands that these residuals exhibit specific characteristics, including symmetry, absence of correlation, adherence to normal distribution, and constant variance.

Shown in Fig.3. are the residuals plots for the response variable  $K$ , revealing that the residuals conform to normal distribution (as evident in the normal probability plot), lack skewness (as demonstrated by the histogram), display no correlation among themselves (as seen in the residuals vs. order plot), and maintain constant variance (as indicated in the residuals vs. fits plot). Indicating that the ordinary least squares method that was used to produce the equation above assumptions are fully satisfied.

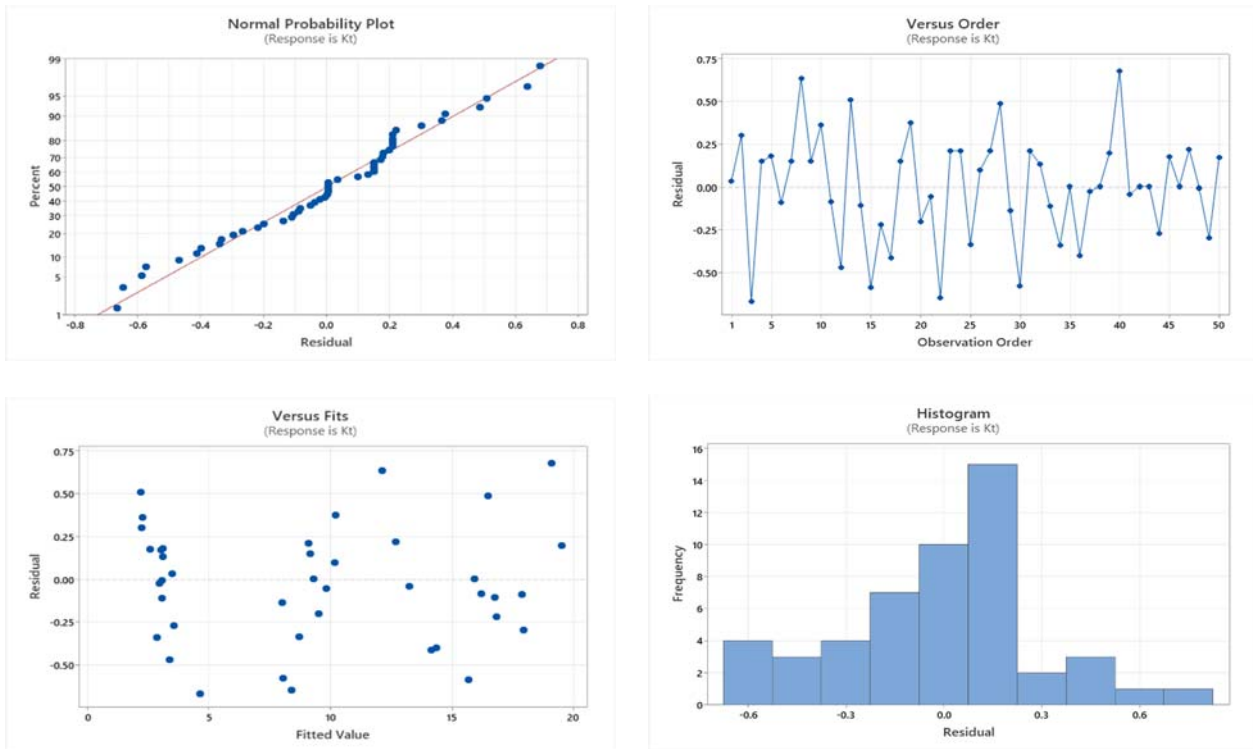


Fig.3. Residual tables for RSM.

### 5.3. Main effects of the geometric parameters

Fig.4. shows the effect that each of the parameters studied  $\left(\frac{r}{w}, \frac{t}{r}, \frac{C_s}{t}, \theta_c, \sigma_r\right)$  on the value of  $K_t$ . The figure shows that  $K_t$  correlates linearly (nearly linear in the case of  $\sigma_r$ ) and positively with each of the studied parameters being influenced the most by the value of  $\left(\sigma_r = \frac{\sigma_y}{\sigma_x}\right)$  and  $\theta_c$  having the least effect.

In summary, the results and data from the Response Surface Methodology (RSM) in this study reliably and accurately predict the stress concentration factor in an isotropic rectangular plate subjected to biaxial loading and featuring a single countersunk rivet hole.

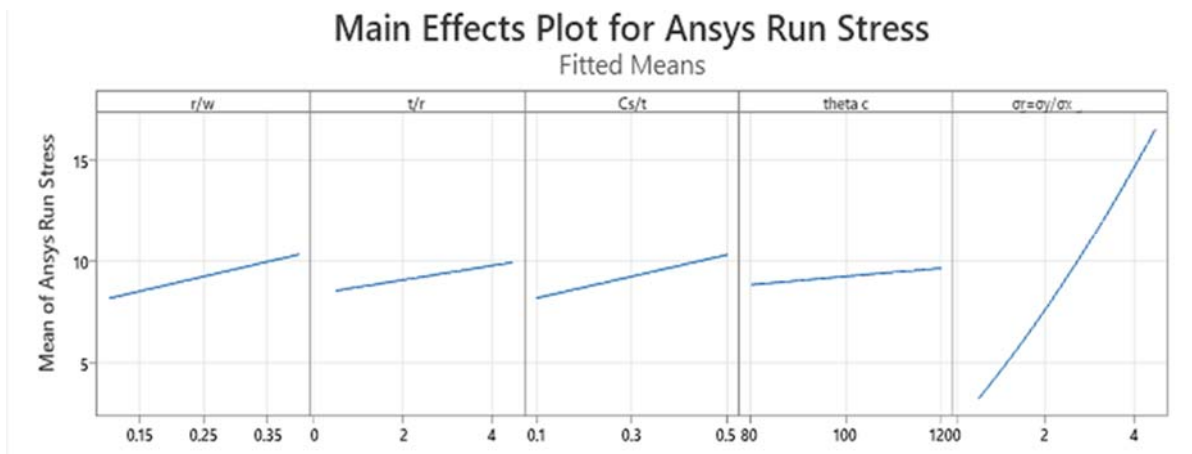


Fig.4. Main effects plot.

## 6. Conclusion

This paper intensively studied the SCF in biaxially loaded isotropic rectangular plates with a centrally placed countersunk hole using finite element and response surface methods. Past papers finding were leveraged to create a more refined model. The influence of five dimensionless geometric and loading parameters  $\left(\frac{r}{w}, \frac{t}{r}, \frac{C_s}{t}, \theta_c, \sigma_r\right)$  on the stress concentration factor  $K_t$  was comprehensively analyzed. A highly effective and accurate second-order equation was reached by using response surface and ordinary least squares methods and was validated with data from finite element analysis. Based on the data presented in this study, we suggest that for any application with similar loading and geometric properties, the ratio between the two loading directions should be as small as possible. Additionally, using smaller radii is recommended for a lower stress concentration factor.

## Acknowledgment

This work was supported by The Hashemite University.

## Nomenclature

$C_s$  – countersink depth

- $\frac{C_s}{t}$  – countersink to thickness ratio  
 $E$  – modulus of elasticity  
 FE – finite element  
 FEA – finite element analysis  
 $K_t$  – stress concentration factor  
 $l$  – plate length  
 $\frac{R}{w}$  – radius to width ratio  
 $R^2$  – coefficient of determination  
 RSM – response surface method  
 $r$  – hole radius  
 SCF – stress concentration factor  
 $t$  – plate thickness  
 $w$  – plate width  
 $\theta_c$  – countersink angle  
 $\nu$  – Poisson's ratio  
 $\sigma_x$  – loading in  $x$  direction  
 $\sigma_y$  – loading in  $y$  direction

## Appendix

Table 2. Analysis of variance.

Source	DF	Adj SS	Adj MS	F-Value	P-Value
Model	15	1327.97	88.53	622.08	0.000
Blocks	2	0.31	0.15	1.07	0.354
Linear	5	1287.30	257.46	1809.08	0.000
r/w	1	30.93	30.93	217.35	0.000
t/r	1	12.92	12.92	90.81	0.000
Cs/t	1	30.34	30.34	213.17	0.000
thetac	1	4.80	4.80	33.74	0.000
Sigma2/Sigma1	1	1229.91	1229.91	8642.11	0.000
Square	1	3.55	3.55	24.94	0.000
Sigma2/Sigma1*Sigma2/Sigma1	1	3.55	3.55	24.94	0.000
2-WayInteraction	7	29.11	4.16	29.22	0.000
r/w*Sigma2/Sigma1	1	14.42	14.42	101.35	0.000
t/r*Cs/t	1	4.07	4.07	28.59	0.000
t/r*thetac	1	0.68	0.68	4.77	0.036
t/r*Sigma2/Sigma1	1	3.23	3.23	22.68	0.000
Cs/t*thetac	1	1.87	1.87	13.17	0.001
Cs/t*Sigma2/Sigma1	1	10.75	10.75	75.51	0.000
thetac*Sigma2/Sigma1	1	1.30	1.30	9.16	0.005
Error	34	4.84	0.14		
Lack-of-Fit	25	4.84	0.19	*	*
PureError	9	0.00	0.00		

Table 3. FEA, RSM, errordata.

Run order	$r/w$	$t/r$	$C_s/t$	$\theta_c$	$\sigma_r$	$K_t$ from ansys	$K_t$ from equations	Error%
1	0.4	0.5	0.5	120	0.5	3.525	3.515	0.271
2	0.1	0.5	0.1	120	0.5	2.555	2.281	10.743
3	0.1	4.5	0.5	120	0.5	3.981	4.676	-17.469
4	0.25	2.5	0.3	100	2.5	9.333	9.211	1.309
5	0.4	4.5	0.1	120	0.5	3.297	3.147	4.557
6	0.4	0.5	0.5	80	4.5	17.806	17.920	-0.639
7	0.25	2.5	0.3	100	2.5	9.333	9.211	1.309
8	0.1	0.5	0.1	80	4.5	12.770	12.160	4.776
9	0.25	2.5	0.3	100	2.5	9.333	9.211	1.309
11	0.1	4.5	0.1	80	0.5	2.640	2.304	12.733
12	0.4	0.5	0.1	120	4.5	16.120	16.232	-0.699
13	0.4	0.5	0.1	80	0.5	2.917	3.415	-17.080
14	0.1	0.5	0.5	80	0.5	2.735	2.252	17.678
15	0.4	4.5	0.1	80	4.5	16.668	16.803	-0.807
16	0.1	0.5	0.5	120	4.5	15.104	15.717	-4.060
17	0.1	4.5	0.5	80	4.5	16.616	16.862	-1.480
18	0.1	4.5	0.1	120	4.5	13.738	14.179	-3.214
19	0.25	2.5	0.3	100	2.5	9.333	9.211	1.309
21	0.4	2.5	0.3	100	2.5	10.585	10.295	2.734
22	0.25	2.5	0.3	120	2.5	9.333	9.620	-3.079
23	0.25	4.5	0.3	100	2.5	9.771	9.912	-1.447
24	0.25	0.5	0.3	100	2.5	7.774	8.509	-9.459
25	0.25	2.5	0.3	100	2.5	9.333	9.211	1.309
26	0.25	2.5	0.3	100	2.5	9.333	9.211	1.309
27	0.25	2.5	0.3	80	2.5	8.378	8.801	-5.049
28	0.25	2.5	0.5	100	2.5	10.297	10.284	0.127
29	0.25	2.5	0.3	100	2.5	9.333	9.211	1.309
30	0.25	2.5	0.3	100	4.5	16.962	16.563	2.351
31	0.1	2.5	0.3	100	2.5	7.901	8.127	-2.855
32	0.25	2.5	0.1	100	2.5	7.473	8.138	-8.893
33	0.25	2.5	0.3	100	2.5	9.333	9.211	1.309
34	0.25	2.5	0.3	100	0.5	3.257	3.213	1.368
36	0.4	0.5	0.1	120	0.5	2.958	2.950	0.253
38	0.1	0.5	0.1	80	0.5	2.524	2.746	-8.793
39	0.4	0.5	0.1	80	4.5	15.947	15.827	0.753
40	0.1	0.5	0.5	80	4.5	13.973	14.253	-2.002
41	0.1	0.5	0.5	120	0.5	2.944	2.846	3.323
42	0.25	2.5	0.3	100	2.5	9.333	9.211	1.309
43	0.4	0.5	0.5	120	4.5	19.705	19.385	1.626
44	0.1	4.5	0.5	120	4.5	19.762	18.965	4.031
45	0.1	4.5	0.1	80	4.5	13.214	13.136	0.593
46	0.25	2.5	0.3	100	2.5	9.333	9.211	1.309
47	0.25	2.5	0.3	100	2.5	9.333	9.211	1.309
48	0.1	4.5	0.5	80	0.5	3.293	3.444	-4.557
49	0.1	4.5	0.1	120	0.5	2.770	2.477	10.577
50	0.25	2.5	0.3	100	2.5	9.333	9.211	1.309
51	0.1	0.5	0.1	120	4.5	12.903	12.565	2.623
52	0.4	4.5	0.1	80	0.5	3.085	2.974	3.597
53	0.4	4.5	0.1	120	4.5	17.666	17.847	-1.023

Table 4 cont. FEA, RSM, errordata.

Run order	$r/w$	$t/r$	$C_s/t$	$\theta_c$	$\sigma_r$	$K_t$ from ansys	$K_t$ from equations	Error%
54	0.4	0.5	0.5	80	0.5	3.213	2.921	9.091
55	0.5	0.1	0.7	120	0.5	3.930	3.756	4.416
56	0.05	6.5	0.3	60	3	9.216	9.241	-0.270
57	0.1	1.5	0.6	160	10	54.879	48.426	11.757
58	0.25	2	0.05	150	2	5.574	6.380	-14.458
59	0.4	3	0.5	84	5	27.553	22.115	19.739
60	0.06	6	0.3	104	3	10.498	10.843	-3.290
61	0.3	3.225	0.1	121	4	13.566	14.176	-4.492
62	0.2	4.5	0.6	111	6	34.827	28.151	19.170
63	0.1	0.5	0.3	60	4	11.623	11.158	4.000
64	0.25	1	0.1	125	1	2.251	3.804	-68.967

## References

- [1] Pilkey W.D., Pilkey D.F. and Bi Z.(2020): *Peterson's Stress Concentration Factors. Fourth edition.*– Hoboken, NJ: John Wiley & Sons, Inc.
- [2] Shivakumar K.N. and Newman J.C. (1995): *Stress concentration equations for straight-shank and countersunk holes in plates.*– Journal of Applied Mechanics, vol.62, pp.248-249.
- [3] Wu H.-C. and Mu B. (2003): *On stress concentrations for isotropic/orthotropic plates and cylinders with a circular hole.*– Composites Part B: Engineering, vol.34, pp.127-134.
- [4] Kotousov A. and Wang C.H. (2002): *Three-dimensional stress constraint in an elastic plate with a notch.*– International Journal of Solids and Structures, vol.39, pp.4311-4326.
- [5] Li Z., Guo W. and Kuang Z. (2000): *Three-dimensional elastic stress fields near notches in finite thickness plates.*– International Journal of Solids and Structures, vol.37, pp.7617-7632.
- [6] She C. and Guo W. (2007): *Three-dimensional stress concentrations at elliptic holes in elastic isotropic plates subjected to tensile stress.*– International Journal of Fatigue, vol.29, pp.330-335.
- [7] Enab T.A. (2014): *Stress concentration analysis in functionally graded plates with elliptic holes under biaxial loadings.*– Ain Shams Engineering Journal, vol.5, pp.839-850.
- [8] Kumar A., Agrawal A., Ghadai R. and Kalita K. (2016): *Analysis of stress concentration in orthotropic laminates.*– Procedia Technology, vol.23, pp.156-162.
- [9] Jadvani N., Dhiraj V.S., Joshi S. and Kalita K. (2017): *Non-dimensional stress analysis of orthotropic laminates.*– Materials Focus, vol.6, pp.63-71.
- [10] Zhou Y. and Fei Q. (2017): *Evaluation of opening-hole shapes for rivet connection of a composite plate.*– Proceedings of the Institution of Mechanical Engineers, Part C: Journal of Mechanical Engineering Science, vol.231, pp.3810-3817.
- [11] Kumar S.A., Rajesh R. and Pugazhendhi S. (2020): *A review of stress concentration studies on fibre composite panels with holes/cutouts.*– Proceedings of the Institution of Mechanical Engineers, Part L: Journal of Materials: Design and Applications, vol.234, pp.1461-1472.
- [12] Whaley R.E. (1965): *Stress-concentration factors for countersunk holes: Method described by the author is based upon the knowledge of the elastic stress-concentration factor of a similar but simple plain-hole configuration.*– Experimental Mechanics, vol.5, pp.257-261.
- [13] Cheng Y.F. (1978): *Stress-concentration factors for a countersunk hole in a flat bar in tension and transverse bending.*– Journal of Applied Mechanics, vol.45, pp.929-932.
- [14] Shivakumar K.N., Bhargava A. and Newman J.C. (2007): *A tensile stress concentration equation for countersunk holes.*– Journal of Aircraft, vol.44, pp.194-200.
- [15] Bhargava A. and Shivakumar K.N. (2008): *A three-dimensional strain concentration equation for countersunk holes.*– The Journal of Strain Analysis for Engineering Design, vol.43, pp.75-85.

- [16] Bhargava A. and Shivakumar K.N. (2007): *Three-dimensional tensile stress concentration in countersunk rivet holes.*– The Aeronautical Journal, vol.111, pp.777-786.
- [17] Darwish F., Gharaibeh M. and Tashtoush G. (2012): *A modified equation for the stress concentration factor in countersunk holes.*– European Journal of Mechanics - A/Solids, vol.36, pp.94-103.
- [18] Darwish F., Tashtoush G. and Gharaibeh M. (2013): *Stress concentration analysis for countersunk rivet holes in orthotropic plates.*– European Journal of Mechanics - A/Solids, vol.37, pp.69-78.
- [19] Gharaibeh M.A. (2020): *A study on the stress concentration factor induced in double countersunk holes due to uniaxial tension.*– International Journal of Applied Mechanics and Engineering, vol.25, pp.59-68.
- [20] Gharaibeh M.A., Tlilan H. and Gharaibeh B.M. (2021): *Stress concentration factor analysis of countersunk holes using finite element analysis and response surface methodology.*– Australian Journal of Mechanical Engineering, vol.19, pp.30-38.
- [21] Bhargava A. and Shivakumar K.N. (2008): *A three-dimensional strain concentration equation for countersunk holes.*– The Journal of Strain Analysis for Engineering Design, vol.43, pp.75-85.
- [22] Hayajneh M., Darwish F.H. and Alshyyab A. (2014): *A modelling strategy and strain concentration analysis for a countersunk hole in an orthotropic plate.*– International Journal of Design Engineering, vol.5, pp.175-192.
- [23] Jeissat M. and Gharaibeh M.A. (2021): *Analysis and optimization of the strain concentration factor in countersunk rivet holes via finite element and response surface methods.*– Multidiscipline Modeling in Materials and Structures, vol.17, pp.537-551.
- [24] Gharaibeh M.A. (2022): *A high-accuracy empirical formula for the strain concentration factor in countersunk holes.*– Mathematical Modelling of Engineering Problems, vol.9, No.3, p.591.
- [25] Gharaibeh M.A. (2023): *Analysis, formulation, and optimization of the strain concentration factor in double countersunk holes due to uniaxial tension.*– Australian Journal of Mechanical Engineering, vol.21, pp.384-392.
- [26] Alshyyab A.S. and Darwish F.H. (2018): *Three-dimensional stress analysis around rivet holes in a plate subjected to biaxial loading.*– Jordan Journal of Mechanical & Industrial Engineering, vol.12, pp.233-242.

Received: June 9, 2024

Revised: December 17, 2024